Journal of Physics Communications

PAPER

A geometry dependent directivity analysis of an optical structure based on NV center in diamond

Subhankar Roy and M Ummal Momeen

Magnetic Instrumentation and Applied Optics Laboratory, Department of Physics, School of Advanced Sciences, Vellore Institute of Technology, Vellore, Tamil Nadu, 632014, India

E-mail: ummalmomeen@gmail.com

Keywords: e-SIL, directivity, geometrical tolerance, ZPL

OPEN ACCESS

RECEIVED
24 October 2023

REVISED
1 January 2024

ACCEPTED FOR PUBLICATION
11 January 2024

PUBLISHED
23 January 2024

Abstract

We present and investigate a highly directional diamond based optical nanostructure embedded with an elliptical solid immersion lens (e-SIL). An in depth analysis of the far field evolution is elucidated with respect to geometrical modification. This design is capable of producing a maximum directivity of ∼11 dB at its optimized position. Geometrical tolerance and directional behavior has been studied within a wide range of dipole variation. The incident light source noise is neutralized with the manipulation of e-SIL geometry by considering an experimental simulation environment. Enhancement in directivity near NV center zero phonon line (ZPL) region with reduced excitation light source noise can improve the overall efficiency of the NV single photon emitter and can be useful for multiple photonic applications.

1. Introduction

Diamond based optical nanostructure devices have unique applications in the quantum communication research [1–3]. The use of these optical structures has reduced the size of quantum networks significantly in the fields of quantum sensing and quantum information processing applications [4, 5]. In the photonics research, stable generation of single photon from quantum emitter is an important requirement for the construction of qubits. Several single photon sources are available such as quantum dot [6, 7], functionalized carbon nanotubes [8], two dimensional materials [9] and solid state defects [10]. Among all nitrogen vacancy (NV^-) centers stands out due to long electronic spin coherence time and highly stable emission even at ambient conditions. The emission spectrum of NV^- consists of a zero phonon line (ZPL) at 637 nm with a broad phonon side band [10] which has a significant contribution in highly sensitive magnetometry applications [11] due to its spin dependent fluorescent emission. Therefore, improvement of directional photon emission towards a collection system at ZPL is critically important.

One of the most seminal parameters of any kind of NV based nanostructure is related to the geometry of that optical structure. A highly directive emission along with stable geometrical tolerance is essential for the construction of efficient nanoantenna design. Hence, the perfect optimization of nanoscale device in terms of geometry is a prerequisite to design optical devices with high photon collection efficiency. Due to high refractive index of diamond, the critical angle is very less at diamond-air interface. This yields very small amount of photons coming towards lower numerical aperture collective lens [12] and minimize the directivity near ZPL. Several research efforts have been adopted to improve directive photon emission adequately.

To resolve this issue, an optical structure has been introduced in combination with diamond substrate i.e. solid immersion lens (SIL) structure or commonly known as SIL based structure. Different optical nanostructures including optical wave guide [13, 14] are being designed with this remarkably simple and straightforward approach [15].

Numerous diamond based SIL structures have been reported [16, 17] to improve photon collection efficiency (PCE) by minimizing the total internal reflection effect at diamond-air interface. Later the sculpture of general hemispherical SIL has been slightly amended to achieve more photon counts from these systems [14].

We focus to minimize the excitation light source noise of the optical nanostructure which in turn predominantly increases the directivity. The directivity of the far field emission profile is expected to be reduced when the NV dipole emitter is excited at a wavelength of 532 nm. An enhancement in PCE (in terms of directivity) for the same optical structure is required in order to improve the performance of the device when it is operated at emission wavelength (637 nm). A dominant emission in both upward and downward direction is observed even after the inclusion of spherical SIL, especially in our optical system. Hence elliptical SIL structure has been adopted to overcome this problem which sends the light beam downwards more directionally [18].

In this work we demonstrate an NV center based optical structure in nanoscale regime. This simpler geometry has been introduced to increase the directivity near ZPL of a NV spectrum. The benefit of our proposed design is that the rectangular diamond box below the SIL acts as a solid cavity and effectively minimizes the backscattered light at diamond box-SIL interface. A detailed comparison of directivity and far field emission pattern starting from excitation wavelength to emission wavelength has been exploited here. Geometrical tolerance of different dipole emitter position also has been presented to check the robustness of this optical structure. In the last part, the evolution of far field under the illumination of a laser beam has been simulated and the noise produced during green light (∼532 nm) excitation is reduced. Outstanding features have been obtained for this optical structure which enables the possibility to explore quantum communication applications.

2. Methods and model descriptions

We employed a three dimensional Finite Element Method calculation to study our optical structure with the help of COMSOL Multiphysics 5.2a software package tool. The complete directivity analysis has been made via wave optics module. Both the rectangular substrate and ellipsoid SIL is made up of high refractive index material i.e. diamond. The outgoing radiation is absorbed by considering a PML layer over the complete system. This will not allow much light beams to reflect back and helps to converge the simulation results. Scattering boundary condition is considered outside the PML layer to override perfect electric conductor (PEC) condition at the outer surface. NV center excitation comes under ∼532 nm wavelength region and it results in a fluorescence emission of ∼637 nm. Hence, we have applied the excitation and emission wavelength as 532 nm and 637 nm respectively. The point dipole in COMSOL environment is used as optical dipole emitter inside the diamond solid immersion lens in order to replicate the NV center defect inside a diamond substrate. The orientation of the dipole emitter is taken along x axis in 2D modeling and x axis on xy plane in 3D modeling which is perpendicular to the diamond N-V axis. The meshing operation is performed by considering a typical finer mesh which can converge the overall simulation and resolves the issue when the dipole is almost near to the surface.

3. Results and discussion

We have simulated the photon emitter based optical nanostructure and studied the following characteristics such as geometry dependence, directivity analysis and tolerance with respect to dipole position to confirm the robustness of the nanorange device. A detailed analysis is presented in the following sub-sections. In addition, we presented the capability of noise reduction during incident light excitation by our optimized structure which provides a significant improvement in the contrast while detecting the output signal. Further, we have also shown the enhancement factor and collection efficiency for our optimized parameters.

3.1. Geometry dependent emission

The theory of SIL concept is given by Born and Wolf [19] where they explain how light can be focused from almost all the directions within a high index spherical structure. Due to refractive index mismatch between air-diamond interface maximum light radiation from a single photon emitter inside a diamond substrate undergoes total internal reflection. Therefore, one cannot detect the maximum photon collection efficiency from a simple bulk diamond substrate. Instead, this ellipsoid SIL along with a cuboid structure eliminates the maximum TIR effect and directs higher number of emitted photons towards collective path which has been considered at the bottom of the structure (figure 1). The prime focus of our work is to excite this complete dielectric nanostructure from the top while the collection of emitted photons is considered towards the bottom of the structure in order to maintain a clear distinction between incident radiation (∼532 nm) and emitted output radiation (637 nm). An in-depth excitation cum detection scheme is shown in figure 1. The fluorescence output at emission wavelength (∼ 637 nm) and the background noise produced due to the incident wavelength (∼532 nm) is collected from the bottom of the structure which is shown through a schematic representation (figure 1).

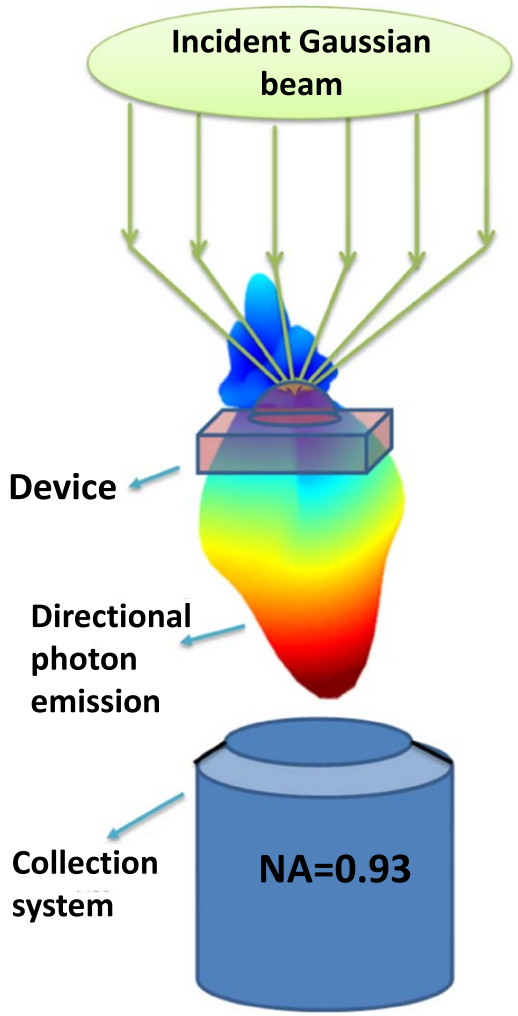

Figure 1. A detailed schematic diagram of photon detection scheme is shown here. The incident excitation and the collection path are indicated in this figure.

Here we predominantly study an elliptical SIL with a slight modification along the principal axis. In the following, we describe a design concept to quantify the important optical property of a nanoantenna i.e. directionality.

Our optimized geometry is a truncated ellipsoid structure. The detailed configuration about the description of our model is given in figure 2(a). We can reliably compare the e-SIL model parameters in 3D with a basic ellipsoid structure where 'a' and 'b' correspond to the semi major axes while h is the height or it represents the semi minor axis of the e-SIL. To clarify in detail, a two dimensional cross sectional view is presented for both the planes (XZ plane and YZ plane) in figure 2(b). Throughout the calculation h parameter is kept as constant and directivity analysis is performed by changing a/b ratio. Here we have considered one parameter 'P' where P denotes the ratio of two semi major axes dimensions such as P = a/b.This e-SIL nanostructure is embedded with a cuboid diamond substrate with a dimension of 1.2 μm × 1.0 μm × 0.5 μm. Light radiation coming from the e-SIL gets reflected back towards the lower NA collective lens due to the rectangular shaped substrate which drastically increases the directionality. During the optimization, we have fixed one semi major axis dimension ('b') to be 250 nm and varied the other dimension ('a') from 250 nm to 500 nm with the interval of 50 nm. The height (h) of the e-SIL is taken as 300 nm. The NV defect is almost placed near the curved surface of the solid immersion lens (50 nm away from the top curved surface of our e-SIL structure) which is shown in figure 2(c).

To better understand the optical structure, a beam propagation simulation is performed where we have explained the benefits of our complete system consideration. Electric field distribution is the fundamental parameter to analyse the performance of different miniaturised devices [20]. Figure 3(a) represents the photon emission direction in the presence of only solid immersion lens structure. A symmetric field distribution along all over the simulation area indicates that there is a significant loss in photon detection towards collection system at the bottom of our structure. Rather, the cuboid embedded e-SIL structure directed more emitted radiation towards collection path without marginal loss due to its solid cavity structure [figure 3(b)]. This shows that the

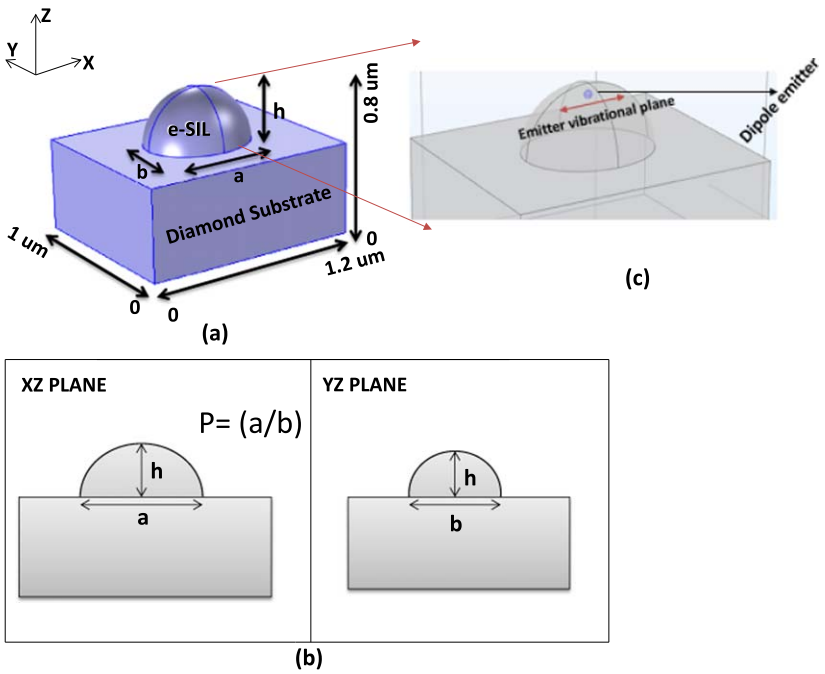

Figure 2. (a) Three dimensional schematic diagram of our optimized model. (b) A two dimensional cross sectional view of the e-SIL for both XZ and YZ plane. (c) Location of the dipole emitter position is shown here.

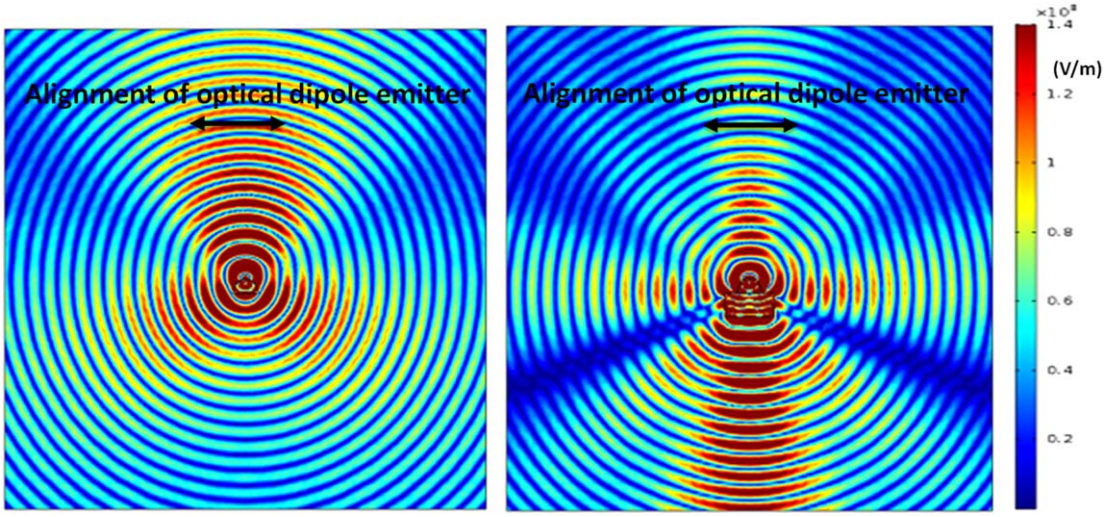

Figure 3. The far field emission profile of our e-SIL and cuboid structure is shown here (a) when only e-SIL structure is considered for NV center emission. (b) The emission profile of our complete system (embedded e-SIL and cuboid structure) is represented in this figure. Both the cases dipole vibration is considered along *x* axis.

geometry parameters play a significant role to direct the beam propagation which is the major variable in our case. Figure 3 justifies that more emitted radiation is propagated towards collection path. Throughout the complete analysis of our structure, we consider the vibrational plane of our dipole emitter (NV center as single photon emitter) along XY plane when it is considered for a 3D model and along x plane when we calculate for a 2D model which is perpendicular to NV- axis inside diamond lattice.

Numerical analysis of far field evolution during the optimization is depicted in figure 4. In these geometry modifications, light emission is heavily dependent on SIL size. Here special attention is given to quantify the far field beam pattern of the antenna towards lower side. Far field analysis is essential for calculating the photon collection efficiency of our optical structure where more directional and collimated emission profile signifies that the photon emission output is quite high. The less intense and scattered beam reduces the emission rate towards collection aperture which in turn reduces the PCE. The far field intensity distribution is relevant to average power distribution calculation which is widely used in photon collection efficiency estimation for optical

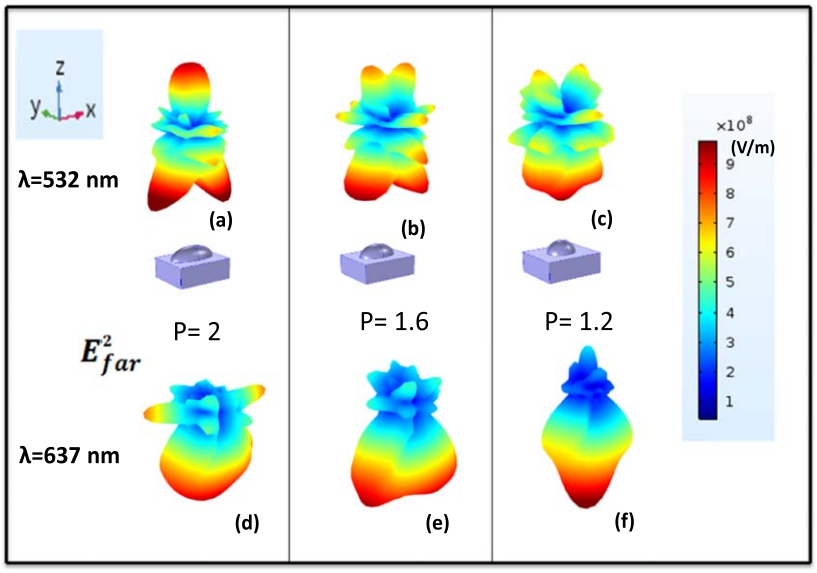

Figure 4. 3D far field evolution of our optimized optical system at 532 nm and 637 nm is shown here. Far field intensity (V/m) ^ 2 versus the variation in P value is plotted. (a) (b) (c) Optimized far field pattern while device is excited at 532 nm and (d) (e) (f) Far field distribution while device is excited at 637 nm. For both the cases, P is considered as 2, 1.6 and 1.2. Maximum directionality occurs at 637 nm excitation when P = 1.2.

nanostructures. So, far field emission pattern needs to be analysed in greater detail. The dimensions of an e-SIL actively affect the average power of a dipole emitter and simultaneously the far filed pattern as well. Furthermore, scattered radiation in lateral direction is also compressed by the optimized geometry parameters of the e-SIL. The dipole vibrational axis has been preferentially considered parallel to the *x* axis (on xy plane) of our three-dimensional model. This dipole orientation facilitates maximum emission to radiate out of the device in order to achieve single dominated lobe towards collective aperture at 637 nm. The value of P (ratio of semi-major axis distances) has been commenced from 2 and ended with 1 in steps of 0.2. In each step, emission profile of the antenna has been observed and plotted in figure 4. Alterations in e-SIL structure causes a change in beam profile at the substrate-SIL interface which plays a crucial role in the radiation pattern at different wavelengths. By optimizing the e-SIL geometry, we eliminate those drawbacks.

This analogy goes even further when we calculate the directionality of our structure under the exposure of both excitation (~532 nm) and emission wavelength (~637 nm). A highly directional light beam is expected as an output at emission wavelength region (~637 nm) while the directionality must be reduced for the incident excitation wavelength (~532 nm) along the output detection path. Initialization of optimization started by considering one of the semi major axes value as 'a' = 500 nm. Figures 4(a), (b) and (c) represent the far field radiation pattern for different geometrical parameters at an operating wavelength of 532 nm. This exhibits multiple high intense side lobes at higher value of P as less number of TIR beams is impinging towards a particular direction. More precisely, the decrement in 'P' value helps to reduce the directionality at 532 nm due to distributed field patterns. This lower directional behavior of far field emission profile intends to prove that less radiation pass through the collection aperture at the bottom when the device is exposed under excitation light source. Simultaneously, the background noise produced by the device in terms of scattered emission at 532 nm is also reduced significantly.

On the other hand, same optimization helps to improve the directionality towards a particular direction (detection path) at emission wavelength. Figures 4(d), (e) and (f) display the directional behavior of our device towards downward direction at 637 nm. Higher number of photon detection within a lower numerical aperture is achieved with this highly collimated and directional far field emission profile. Due to wider 'a' of semi major axis, the reflected beams traverse a broad range of far field area which is shown in figure 4(d). Reduction of P value from 2 to 1.2 reduces the dimensions of semi major axis as well. Indeed, the far field beam profile with lower P value present a narrow and highly directional light emission. This produces a highly collimated far field intensity pattern within our collection aperture at 637 nm (figure 4(f)). From the above discussion, we conclude that our optimized device generates a less intense emission profile with lower directionality when it is excited with a green (~532 nm) laser beam. This predominantly nullifies the photon emission rate produced by the incident excitation light source (~532 nm), that is considered as noise while detecting the fluorescence emission within a given aperture (lower NA). At the same time, the optimized design is capable of producing a directional single lobe with enhanced directionality at 637 nm excitation. The advantage of this far field radiation pattern is

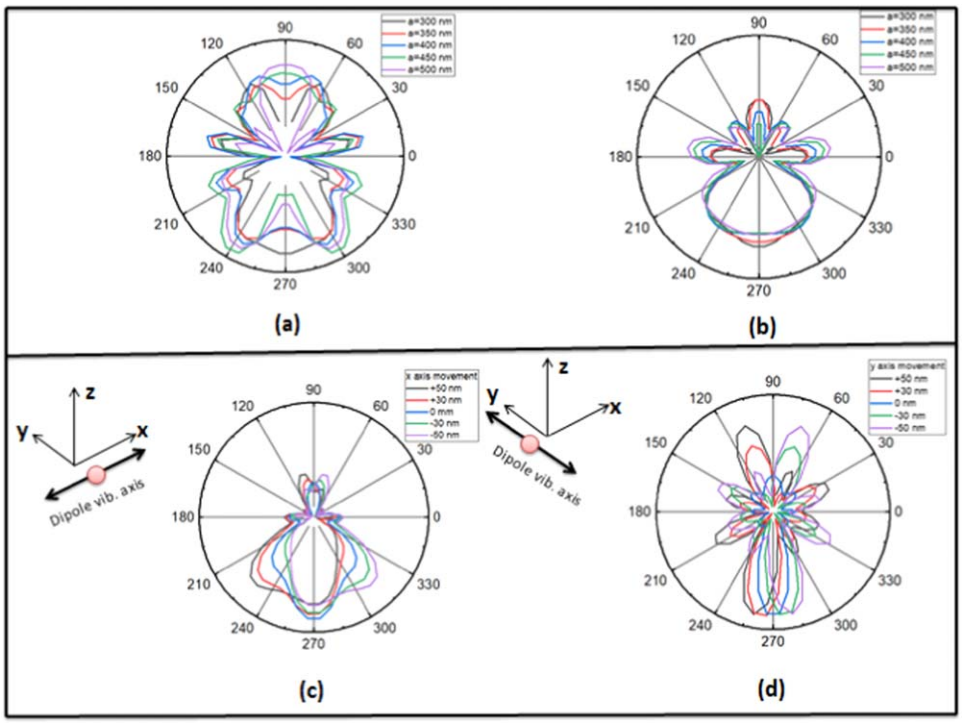

Figure 5. (a) Directivity polar plot when the modification is performed at 532 nm. (b) At 637 nm. (c) In 3D model, there are three different dipole orientations. Here dipole is shifted from −50 nm to + 50 nm along X axis; (d) here dipole is shifted from −50 nm to + 50 nm along Y axis.

that it allows us to understand the directional characteristics of nanoantenna with an intuitive e-SIL model which is discussed in the next section.

3.2. Directivity analysis of optical structure

To enumerate the directionality of optical structure we introduce a formula to measure the directivity [21, 22]. As we have earlier discussed the directionality is the measure of emission intensity distribution towards a given direction, this quantity (directivity) directly implies to the improved photon emission within a defined numerical aperture. Higher directivity value of the optical nanostructures inherently related to higher photon collection efficiency generated by that particular structure. In this case, the directivity demonstrates how the emission profile evolves towards our collection aperture when the dipole emitter is getting exposed under different wavelength illuminations. The directivity can be defined as the ratio between the maximum radiation intensity in a given direction and the average radiation intensity for overall direction coming from the antenna. Maximum directivity towards a particular direction is quantified as,. $D_{\max} = \frac{U_{\max}}{U_0} = \frac{4\pi U_{\max}}{P_{rad}}$

where, $U_{\max}$ is the maximum radiation intensity (W/unit solid angle), U_0 is the average value of radiation intensity and P_{rad} is the total average radiated power delivered from the system.

Now if we express the directivity in dB, then

$$D_{\max} = 10^{*}\log 10\left(\frac{4\pi U_{\max}}{P_{rad}}\right) dB.$$

The correlation between directivity and photon collection efficiency is quite straight forward in terms of power distribution function. The amount of power radiated towards a particular direction out of overall power distribution within a specified numerical aperture is commonly used while calculating the photon collection efficiency value for any optical nanostructure.

3.2.1. Geometry dependent analysis

As shown in figure 5, the emission profile (directionality) can be guided by controlling the geometrical parameters which in turn improves the directionality of fluorescence emission towards the collection path. So, it is highly important to define directivity with respect to geometry variation in this context. Nevertheless, in order to check the performance of our proposed structure we calculated the directivity value by varying the geometrical parameters. A significant improvement in directivity is obtained in our optimized structure. In the previous section (figure 4), we evaluated the far field emission profile by varying P value and finally we obtained a

highly collimated emission profile at optimized position. Same analogy has been followed here in terms of directivity calculation in order to achieve higher efficiency through our optimized device. We have compared both the results at two different operating wavelengths (532 nm and 637 nm) with respect to geometry and presented that our proposed structure produces a maximum gain (at 637 nm). The variation in the P value (or a/b ratio) considerably influence the antenna directivity. As the purpose of the device is to minimize the noise at 532 nm, so we optimized the geometry to reduce the directivity for 532 nm excitation. A decrement in directivity is clearly seen at our optimum design which is around 6.9 dB (for ∼532 nm), which is shown in figure 5(a). Gradually the reduction in directivity value is perceived with a decrement in 'a' parameter at incident excitation wavelength. Figure 5(b) shows the directivity for different semi-major axis distance at 637 nm. The highest directivity reaches a value of 10.9 dB for the optimized model at the wavelength of ∼637 nm. Optimum design confirms a maximum collimated and directional photon emission obtained by our optical nanoantenna.

Our optimized design exhibits almost strong emission within a narrow solid angle regime (figure 5(b)). Higher directionality from the bottom of the system is clearly observed. This result matches with our expected outcome i.e. single lobe emission towards downward direction in far field intensity pattern (a = 300) [figure 5(b)].

This e-SIL parameters' dependence is a direct consequence of ray propagation inside our optimized model. Here smaller value of semi major axis distance leads to the dipole emission within a narrow solid angle after the incident excitation and hence generates a higher directive emission. On the other hand, as our e-SIL and cuboid structure consists of high refractive index material, the effect of wavelength during excitation and emission of NV center will cause a significant change in directivity. Even the emission profile of this optical device fluctuates with a small modification in operating wavelength. To rectify this drawback, model requires a perfect arrangement in geometry which is provided by our optimized structure.

3.3. Tolerance with respect to dipole position

To construct such nano ranged optical structure, geometrical tolerance for the NV center location should be firmly established. Here the impact of different dipole positions on our far field intensity pattern is investigated. The variation in intensity pattern should be taken into account to confirm the tolerance limit. As because of our structure maintain a 3D symmetry and the dipole emitter vibrational plane is considered along xy plane, so it is essential to verify the behavior of emission when the dipole is oscillated along *y* axis at xy plane of our model. Therefore, tolerance test is performed at two different alignments i.e. one along *x* axis and the other along *y* axis and for both the cases dipole orientation is perpendicular to N-V axis which satisfies the NV center modelling in diamond substrate. Figure 5(c) displays the far field pattern which is not deflecting much from the optimized position. Overall the dipole emitter position has been varied from −50 nm to +50 nm which is important for nanoscale device fabrication within the error of ± 50 nm. Directivity value for this variation is computed and provides a maximum deviation of ± 1.5 dB from the optimized value. The far field pattern in polar plot is shown for XZ plane as the dipole has moved with an overall distance of 100 nm along *X* axis. Figure 5(d) represents the variation of far field intensity pattern along YZ plane and it shows good tolerance over a wider dipole variation. Here also the directivity values are not significantly changed during the movement of dipole position. Extreme shift at ± 50 nm provides a deviation of ± 2 dB. As a result, enough tolerance is being obtained for practically implementing this simulation concept into device fabrication.

In case if we move the dipole more than ± 50 nm along all directions, then there will be broader emission pattern with a widespread directivity plot. This results in less collection of photon emission within a smaller numerical aperture lens. Hence in our optimized device parameters, it is suitable to go for ± 50 nm tolerance limit.

3.3.1. Wavelength dependent analysis

The impact of wavelength variation on the directivity of antenna is illustrated in figure 6. The complete parametric sweep is performed within a wavelength range between 500 nm and 700 nm for the optimized parameters (a = 300 nm, b = 250 nm, and h = 300 nm).

Figure 6 shows that our model generates comparatively less directive emission when the dipole is excited within a wavelength range between 500 nm and 600 nm due to scattered light beams from all over the device. Hence the gain of optical antenna is significantly less near lower wavelength regime. The average directivity produced by the optimized antenna fluctuates between 6 dB and 8 dB within 500 to 600 nm. Rather, the enhancement in the characteristic plot implies an inflated directive emission near higher wavelength regime (i.e., between ∼600 nm and 670 nm).

Since, NV center in diamond shows single photon emission near zero phonon line (∼637 nm) of NV spectrum; the ideal directionality is expected at ZPL wavelength. We achieved a maximum directivity value of about ∼11 dB at $\lambda = 637$ nm which is one of the foremost purposes of our work.

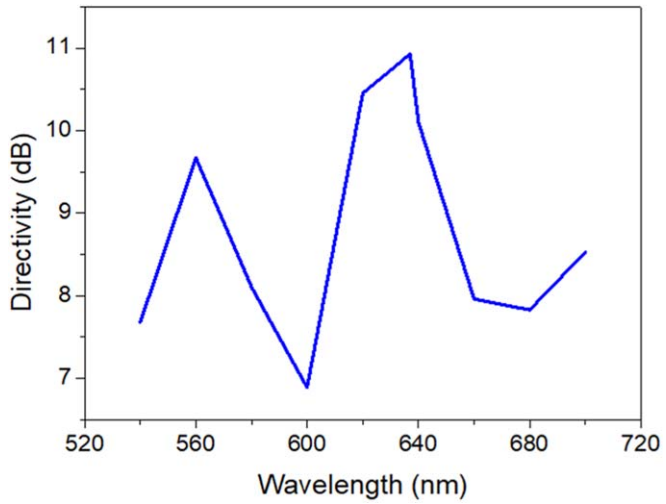

Figure 6. Wavelength versus directivity plot. Maximum Directivity is achieved near ZPL line. Maximum directivity calculated for the optimized system is shown in this plot.

3.4. Noise reduction under laser illumination

In this scheme, we quantitatively discuss the noise suppression technique by our device when it is placed under a green laser excitation (~532 nm) to excite NV center during the output fluorescence detection to show a realistic picture. In any kind of antenna applications, signal to noise ratio (SNR) is a crucial parameter to test the performance of the device. We can increase the gain of our optical waveguide structure while detecting fluorescence emission through the collection path by reducing the incident light excitation (~532 nm) noise. Here in the simulation, we made a structure to mimic a lens to focus the incident light beam (~532 nm) in to the waveguide. The input Gaussian beam has to be converged in such a way that the focal point of the laser beam should coincide with the NV center optimized position.

3.4.1. Electric field distribution of background noise

We employed a simulation to demonstrate the electric field distribution when the antenna is excited with a green laser beam (~532 nm). To apply the laser pulse as an input we construct a Gaussian beam which is focused on to the dipole emitter position. Different virtual numerical apertures have been set to launch the Gaussian beam accordingly. For our study, the applied Gaussian beam radii have been chosen as 700 nm, 1500 nm, 3000 nm and 4000 nm respectively.

The noise generated after the excitation of NV center by the Gaussian laser input pulse at 532 nm is reported in figure 7. Here, we presented a two dimensional cross sectional view of the background noise produced by the structure when it is exposed under a green light illumination for different beam waist in terms of electric field distribution. The variation in electric field intensity distribution for different beam waist ($W_0 = 0.7$ μm, 1.5 μm, 3 μm and 4 μm) are described in figures 7(a),(b),(c),(d) respectively. Due to the limitation of our device dimension, the overall optimization has been accomplished by considering a lower beam waist i.e. 0.7 μm.

A directional beam profile from our optimized structure produces a large amount of photon emission in terms of power (considered as signal) within a specified aperture. To increase the performance/gain of our optical antenna efficiently, signal to noise ratio (SNR) should be quantified. The ratio of the signal and noise power is quantified in terms of SNR. Here we have demonstrated the improvement in SNR while varying different signal intensity (from the NV dipole emission at 637 nm) in comparison with the input Gaussian excitation beam intensity (at 532 nm). The calculation of detected power for both the noise and signal has been computed within a NA of 0.93. SNR = (Average signal power coupled within a given aperture) / (Average noise power coupled within a given aperture).

Figure 8(a) shows the influence on the SNR value when the output dipole signal strength is varied with respect to incident Gaussian illumination for our optimized model. A signal to noise ratio (SNR) of 26 is obtained when an output dipole intensity strength reduces to 0.0215 × 10^−9 (A/m).

We have calculated the enhancement factor for our optimized design and the results are shown in figure 8(b). The ratio between the amount of power delivered from our optimized system and the amount of power delivered by the bulk diamond substrate within a specified collection aperture (NA = 0.5) is defined as the enhancement factor of our model. The sharp enhancement near fluorescence emission output region (~637 nm) proves that our optimized device with e-SIL structure is capable of showing better performance near

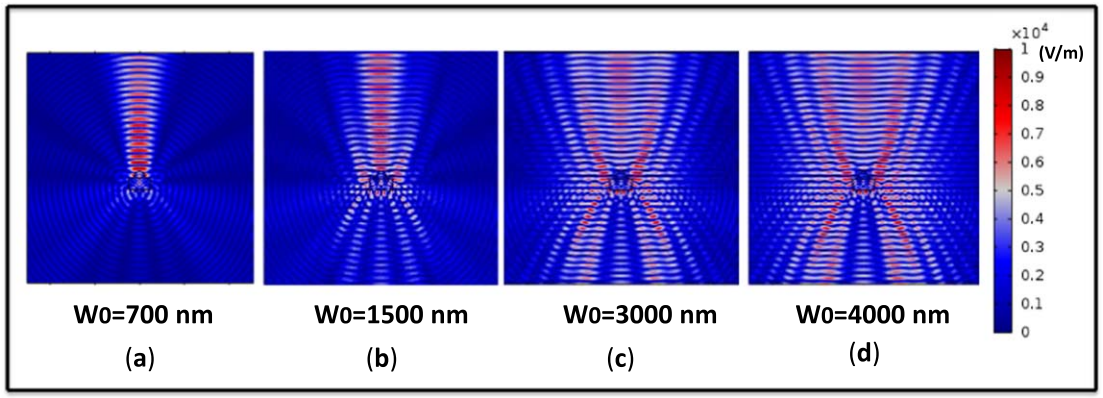

Figure 7. Background noise produced by the structure in terms of electric field distribution of the optimized structure after excitation at 532 nm for different beam radius of applied Gaussian beam (a) $w_0 = 700$ nm, (b) $w_0 = 1500$ nm, (c) $w_0 = 3$ μm and (d) $w_0 = 4$ μm. The simulation area has been considered as 10 μm × 10 μm.

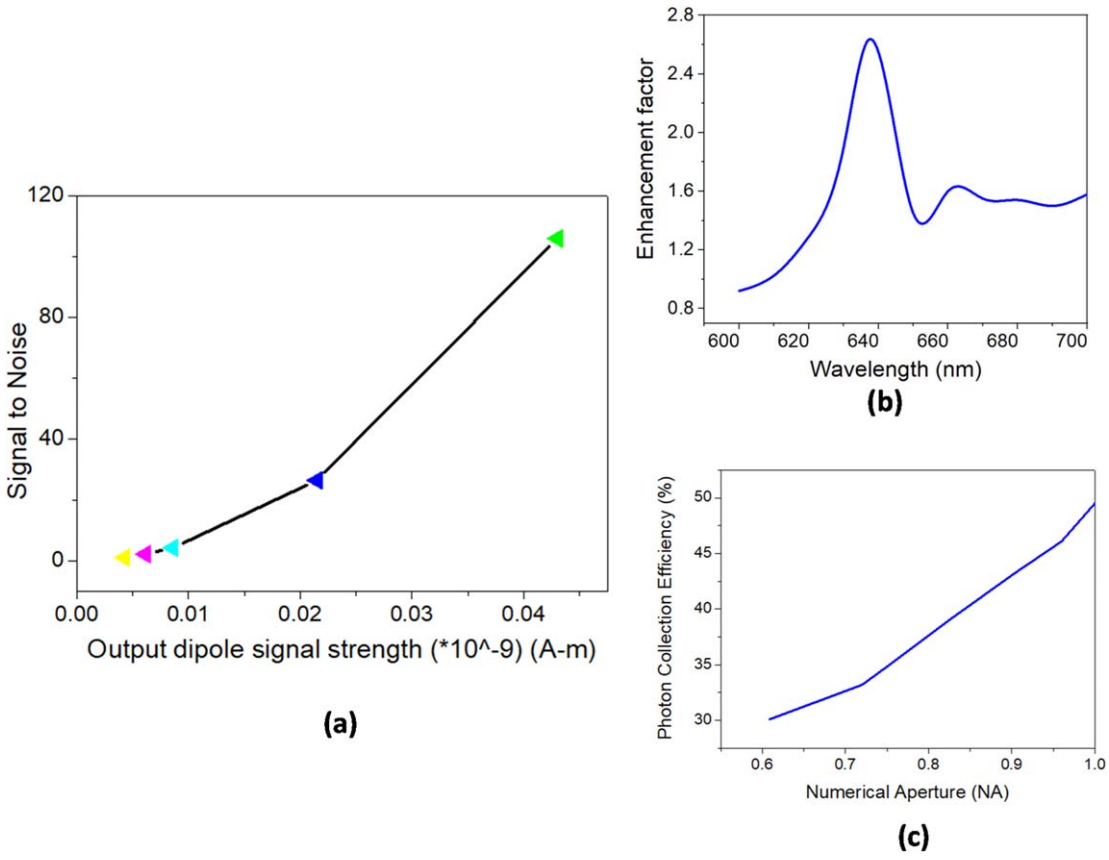

Figure 8. (a) Variation in SNR value with respect to different dipole strength. (b) Here we presented the enhancement factor for our optimized model. (c) Characteristics of photon collection efficiency versus NA of collective lens.

ZPL region compare to ordinary bulk diamond substrate. We have presented a comprehensive comparison of the photon collection on the surface of collective lens with different NA starting from 0.6 to 1 at the emission wavelength of 637 nm. We define the collection efficiency as a ratio between average power distribution within a volume of specified NA and the total average power radiates from the antenna all over the space. Obviously, the PCE value at 637 nm justifies the high performance of our device from the NV emission characteristics point of view. The shape of the e-SIL straightaway proliferate more number of photons within the collective lens yielding higher collection efficiency. Maximum collection efficiency (~50%) is obtained when the semi major axes distance ('a' and 'b') of the e-SIL are considered as 300 nm and 250 nm respectively (figure 8 (c)). Due to the high refractive index of diamond we can collect less number of photons. However, as our antenna is completely

geometry dependent, we considered the collection path of the emission through the bottom of the antenna and reasonably good amount of photon collection is obtained via optimization. Minimum loss is achieved by this optimum structure which is supported by the directional emission at 637 nm. Due to this distinct incident excitation (top of the substrate) and collection path (through the bottom of the substrate), this can be utilized in the experimental setup for introducing additional optical accessories necessary for specific applications.

4. Conclusions

We have simulated an NV based optical structure with embedded ellipsoid SIL structure. Three dimensional electric far field distributions are observed in FEM calculations and it is showing significant improvement in terms of directivity and SNR of the optical structure. Modification in far field emission is demonstrated by changing the (a/b) ratio in principle axes of our e-SIL. The dipole variation over a wider range has been studied for our optimized structure which gives the minimum deflection of directivity (D) value; hence it can provide flexibility in the geometrical tolerance of the device. We have calculated the directivity over a wide range of wavelength and maximum directivity (almost ∼11 dB) is achieved near ZPL line of NV spectrum. Finally, comparison of noise produced by the device during excitation under the illumination of a laser beam is modeled for different optimization stages. The clear distinction between incident and collection path with reduced background noise have made our optical device unique. This highly directional emission with stable geometrical tolerance limit of our device can be useful in the fields of quantum information and quantum sensing areas of research.

Acknowledgments

The authors acknowledge DST-SERB (grant no. EMR/2016/005575), SERB-POWER grant (grant no. SPG/2021/002905) for financial assistance. The authors acknowledge Prof. Jianping Hu for technical discussions.

Data availability statement

The data cannot be made publicly available upon publication because no suitable repository exists for hosting data in this field of study. The data that support the findings of this study are available upon reasonable request from the authors.

ORCID iDs

M Ummal Momeen https://orcid.org/0000-0002-0403-0501

References

[1] Rogobete L, Kaminski F, Agio M and Sandoghdar V 2007 Design of plasmonic nanoantennae for enhancing spontaneous emission *Opt. Lett.* **32** 1623–5
[2] Chu X-l, Brenner T J K, Chen x-w, Ghosh Y, Hollingsworth J A, Sandoghdar V and Götzinger S 2014 Experimental realization of an optical antenna designed for collecting 99% of photons from a quantum emitter *Optica* **1** 203–8
[3] Yousefi L and Foster A C 2012 Waveguide-fed optical hybrid plasmonic patch nano-antenna *Opt. Express* **20** 18326–35
[4] Chen J, Pearlman A J, Ling A, Fan J and Migdall A 2009 A versatile waveguide source of photon pairs for chip-scale quantum information processing *Opt. Express* **17** 6727–40
[5] Scheuer J 2016 Quantum and thermal noise limits of coupled resonator optical waveguide and resonant waveguide optical rotation sensors *J. Opt. Soc. Am.* **33** 1827–34
[6] Michler P, Kiraz A, Becher C, Schoenfeld W V, Petroff P M, Zhang L, Hu E and Imamoglu A 2000 A quantum dot single-photon turnstile device *Science* **290** 2282–5
[7] Javadi A *et al* 2015 Single-photon non-linear optics with a quantum dot in a waveguide *Nat. Commun.* **6** 1–6
[8] Ma X, Hartmann N F, Baldwin J K S, Doorn S K and Htoon H 2015 Room-temperature single-photon generation from solitary dopants of carbon nanotubes *Nature Nanotech* **10** 671–5
[9] Tonndorf P, Schmidt R, Schneider R, Kern J, Buscema M, Steele G A, Gomez A C, van der Zant H S J, de Vasconcellos S M and Bratschitsch R 2015 Single-photon emission from localized excitons in an atomically thin semiconductor *Optica* **2** 347–52
[10] Jelezko F and Wrachtrup J 2006 Single defect centres in diamond: a review *Phys. Status Solidi* **203** 3207–25
[11] Cai J, Jelezko F and Plenio M 2014 Hybrid sensors based on colour centres in diamond and piezoactive layers *Nat. Commun.* **5** 1–6
[12] Le Sage D, Pham L M, Bar-Gill N, Belthangady C, Lukin M D, Yacoby A and Walsworth R L 2012 Efficient photon detection from color centers in a diamond optical waveguide *Phys. Rev.* **85** 121202
[13] Terris B D, Mamin H J, Rugar D, Studenmund W R and Kino G S 1994 Near-field optical data storage using a solid immersion lens *Appl. Phys. Lett.* **65** 388–90
[14] Barnes W L, Bjork G, Gérard J M, Jonsson P, Wasey J A E, Worthing P T and Zwiller V 2002 Solid-state single photon sources: light collection strategies *Eur. Phys. J. D* **18** 197–210

[15] Serrels K A, Ramsay E, Dalgarno P A, Gerardot B D, O'Connor J A, Hadfield R H, Warburtonc R J and Reid D T 2008 Solid immersion lens applications for nanophotonic devices, *J. Nanophotonics* **2** 1–29
[16] Hadden J P, Harrison J P, Stanley-Clarke A C, Marseglia L, Ho Y L D, Patton B R, O'Brien J L and Rarity J G 2010 Strongly enhanced photon collection from diamond defect centers under microfabricated solid immersion lenses *Appl. Phys. Lett.* **97** 241901
[17] Rogers L J *et al* 2014 Multiple intrinsically identical single-photon emitters in the solid state *Nat. Commun.* **5** 4739
[18] Schell A W, Neumer T and Benson O 2014 Numerical analysis of efficient light extraction with an elliptical solid immersion lens *Opt. Lett.* **39** 4639–42
[19] Born M and Wolf E 2002 *Principles of Optics* (London: Cambridge University Press) (https://doi.org/10.1017/CBO9781139644181)
[20] Xu K 2021 Silicon electro-optic micro-modulator fabricated in standard CMOS technology as components for all silicon monolithic integrated optoelectronic systems *J. Micromech. Microeng.* **31** 054001
[21] Bharadwaj P, Deutsch B and Novotny L 2009 Optical antennas *Adv. Opt. Photon.* **1** 438–83
[22] Arisheh A A, Mikki S and Dib N 2020 A Subwavelength-laser-driven transmitting optical nanoantenna for wireless communications *IEEE Journal on Multiscale and Multiphysics Computational Techniques* **5** 144–54